Capturing Conformation-Dependent Molecule–Surface Interactions When Surface Chemistry Is Heterogeneous

Joshua N. Mabry, Mark Kastantin, and Daniel K. Schwartz*

Department of Chemical and Biological Engineering, University of Colorado Boulder, Boulder, Colorado 80309, United States

ABSTRACT Molecular building blocks, such as carbon nanotubes and DNA origami, can be fully integrated into electronic and optical devices if they can be assembled on solid surfaces using biomolecular interactions. However, the conformation and functionality of biomolecules depend strongly on the local chemical environment, which is highly heterogeneous near a surface. To help realize the potential of biomolecular self-assembly, we introduce here a technique to spatially map molecular conformations and adsorption, based on single-molecule fluorescence microscopy. On a deliberately patterned surface, with regions of varying hydrophobicity, we characterized the conformations of adsorbed helicogenic alanine-lysine copeptides using Förster resonance energy transfer. The peptides adopted helical conformations on hydrophilic regions of the surface more often than on hydrophobic regions, consistent with previous ensemble-averaged observations of α-helix surface stability. Interestingly, this dependence on surface chemistry was not due to surface-induced unfolding, as the apparent folding and unfolding dynamics were usually much slower than desorption. The most significant effect of surface chemistry was on the adsorption rate of molecules as a function of their initial conformational state. In particular, regions with higher adsorption rates attracted more molecules in compact, disordered coil states, and this difference in adsorption rates dominated the average conformation of the ensemble. The correlation between adsorption rate and average conformation was also observed on nominally uniform surfaces. Spatial variations in the functional state of adsorbed molecules would strongly affect the success rates of surface-based molecular assembly and can be fully understood using the approach developed in this work.

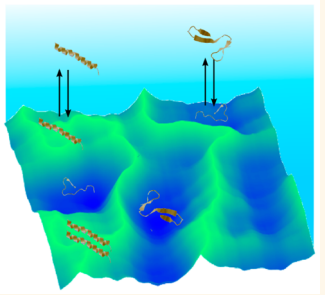

KEYWORDS: single-molecule · α-helix · hydrophobicity · self-assembly · surface chemistry

Biological recognition mechanisms, such as DNA hybridization and antibody–antigen binding, can be exquisitely selective and enable facile assembly of nanodevices[1−3] and programmable materials.[4−6] The specificity of the biomolecular interactions arises because the interacting molecules adopt well-defined secondary structures, such as α-helices in the case of coiled-coil peptide interactions.[7] If biomolecule secondary structure can be retained in the vicinity of a surface, then device building blocks can be reliably positioned and oriented on solid planar substrates via biomolecular recognition.[8,9] Many important sensing mechanisms also rely on biomolecular interactions at interfaces, for example in DNA and peptide microarrays.[10,11] However, the structure of biological macromolecules near interfaces can be different from the bulk structure due to confinement effects and also can be sensitive to surface chemistry.[12−15] Surface-induced effects on biomolecule conformation present a challenge to the bottom-up assembly of hierarchical devices on solid substrates because most of our understanding of biomolecular interactions is based on solution measurements.[16,17] Furthermore, while solutions are relatively homogeneous, solid surfaces are very heterogeneous chemical environments due to variations in local surface chemistry[18,19] and interfacial structuring of the solvent.[20−22] Lateral heterogeneity of surface chemistry presents a particularly difficult challenge to the self-assembly of large-scale devices.

The detailed chemical microenvironment in technologically and biologically important systems is generally unknown *a priori*, and so there is an acute need for methods that can study the dynamics of molecules while properly accounting for environmental heterogeneity.[23] For surfaces, a variety of chemical imaging techniques exist,[24] and low-throughput scanning probe measurements can examine the conformations of relatively static molecular species.[8,25,26]

* Address correspondence to daniel.schwartz@colorado.edu.

Received for review April 7, 2015 and accepted June 16, 2015.

Published online June 16, 2015
10.1021/acsnano.5b02071

© 2015 American Chemical Society

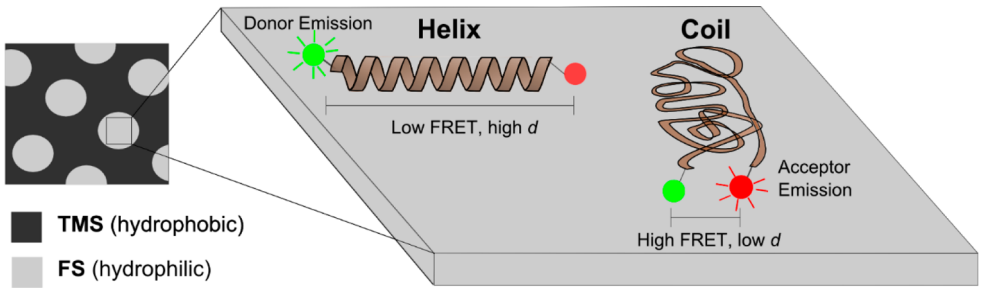

Figure 1. Schematic of mapping technique. On a heterogeneous surface with defined hydrophobic trimethylsilyl (TMS) and hydrophilic fused silica (FS) regions, single molecule observations were accumulated in specific regions (pixels). Peptide end-to-end distance *d* was identified by Förster resonance energy transfer (FRET) between a donor dye at the N-terminus and an acceptor dye at the C-terminus. The end-to-end distance was large for a peptide in the helix state, resulting in low FRET efficiency; for the majority of possible coil conformations, the end-to-end distance was shorter, resulting in high FRET efficiency. The conformations of adsorbed peptides depicted in this scheme are idealized representations for illustrative purposes.

Here, we present a unified technique, based on single-molecule total internal reflection fluorescence microscopy (smTIRFM), for simultaneously mapping a surface and extracting thousands of highly dynamic, single-molecule observations from distinct regions that are identified. This approach is an extension of the previously developed technique, known as mapping using accumulated probe trajectories (MAPT). MAPT can distinguish different regions of a surface based on the dynamics of probe molecules, including adsorption, desorption, and interfacial diffusion.[27] We have extended MAPT imaging to use molecular conformation (specifically molecular end-to-end distance) as a measure of surface functionality. Our MAPT images provide deep insight into conformational dynamics of adsorbed macromolecules on heterogeneous surfaces. We measured relative end-to-end distances for adsorbed molecules using Förster resonance energy transfer (FRET), which is sensitive to distance changes over the 1−10 nm range.[28] To validate our approach, we correlated observations on a deliberately patterned surface with those on uniform surfaces of the same surface chemistries. The molecular probe was a helicogenic peptide, which freely adsorbed onto hydrophilic fused silica (FS) and hydrophobic trimethylsilyl (TMS) surfaces. This particular combination of surface chemistries can be patterned with e-beam lithography and has been used to direct interfacial assembly of biomolecular building blocks, including DNA origami.[8,29,30] More generally, by developing a new spatially resolved, single-molecule technique to study molecular conformation, we can better understand the effect of surface heterogeneity on the structure of freely adsorbing molecules.

RESULTS AND DISCUSSION

Peptide Conformation in Solution and on the Surface. We examined the conformation of short adsorbed peptides, rich in alanine with lysine residues included to confer solubility (specific sequence given in Methods). Peptides with such sequences are known to be strong α-helix formers in solution.[31,32] As depicted in Figure 1, the peptide was end-labeled with donor dye (HiLyte Fluor 488) on the N-terminus and acceptor dye (HiLyte Fluor 594) on the C-terminus so that, upon excitation of the donor dye, the end-to-end distance could be monitored with FRET. To characterize the solution conformation of the peptide, we performed circular dichroism (CD) spectroscopy of the peptide solution and found that the spectra could be fit reasonably well using a linear combination of α-helix and coil reference spectra (Figure S-1). Based on this fit, we estimated that the ensemble-averaged α-helical content of the peptides in solution was ~40% at room temperature. The conformational heterogeneity of alanine-rich helical peptides has been an active area of both theoretical and experimental research over the last two decades.[31−41] A broad distribution of conformations exist at intermediate fractional helicities for peptides that are approximately 20 residues in length, and the kinetics of the conformational state transitions are strongly sequence-dependent.[36,40,41] However, the two-state approximation of single-helix structures in equilibrium with coil structures is widely accepted.[33,36,38] Importantly, atomistic simulations show that the average end-to-end distance for the single-helix population is significantly longer than the average-end-to-end distance for the coil population, even with some fraying of the helix ends, at temperatures where the overall helical content is approximately 40%.[33]

Adsorption of a peptide to a solid surface changes the free energy landscape with respect to molecular conformation. For example, hydrophilic silica surfaces, which are negatively charged at neutral pH,[19] can stabilize helical conformations of peptides containing positively charged residues such as lysine through electrostatic interactions.[42,43] In contrast, the helical content of peptides generally decreases upon adsorption to hydrophobic materials, such as carbon nanotubes,[16,44,45] unless the peptide has been carefully designed to be amphiphilic.[46,47] For many proteins, including bovine serum albumin and fibrinogen, more

secondary structure is lost upon adsorption to hydrophobic surfaces than to hydrophilic surfaces,[48−50] which may also explain why adsorption is much more favorable on hydrophobic surfaces.[51−53] Therefore, we expected a hydrophilic silica surface to favor helical peptide conformations and a hydrophobic surface to destabilize the helix.

Using smTIRFM, we observed peptides freely adsorb to and desorb from each surface, across a field of view (FOV) of $\sim 10^3\ \mu m^2$. In an initial set of screening experiments we captured image sequences of multiple FOV on several samples of each type. An analysis of the trajectories found that they were qualitatively similar and suggested that, in order to achieve sufficiently high resolution, we would be required to accumulate a massive number of trajectories in a particular FOV. Accordingly, a second set of experiments was performed, where we chose one representative FOV on each type of sample and performed long experiments where we captured at least 10^5 trajectories. These image sequences were used for the detailed analysis presented below. During the experiments, we recorded in separate channels the fluorescence intensities of the FRET donor and acceptor dyes, which were spectrally well-separated and were denoted as F_D and F_A, respectively. Single-molecule fluorescence intensity measurements were converted to relative end-to-end distance, $d = (F_D/F_A)^{1/6}$ based on FRET theory.[28] In the Methods section, we detail the theoretical relationship between d and absolute end-to-end distance. In short, d is approximately equal to the absolute end-to-end distance divided by a distance on the order of the Förster radius (~5 nm). We imaged peptides adsorbed on hydrophilic FS, hydrophobic TMS (water contact angle of 91° ± 1°), and photopatterned TMS/FS surfaces. The patterned TMS/FS surface had with ~6 μm diameter FS holes every ~13 μm on a square grid.

To investigate the effect of surface chemistry on peptide structure, we examined the end-to-end distance distributions of the adsorbed helicogenic peptide on surfaces of varying hydrophobicity. The probability distributions of observed d-values (Figure 2A) had similar features on all the surfaces studied. While many molecules had intermediate d-values between 0.4 and 1.8 (i.e., the fluorescence intensity of both the donor and acceptor dye was significant), some molecules had extremely high or extremely low apparent d-values, as represented by rectangular bins at the ends of the distributions in Figure 2A. This measurement artifact largely stemmed from the difficulty of quantifying single-molecule FRET when fluorescence intensity in one channel was very low. Thus, the most salient information available from these d-distributions was the frequency of low d-values compared to the frequency of high d-values, that is, the height of the low d peak (centered at $d = 0.8$) and the height of the high d peak (centered at $d = 1.5$). The low

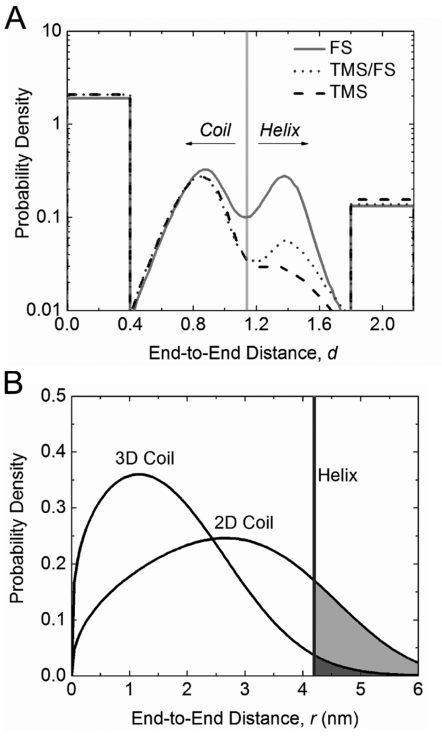

Figure 2. (A) Peptide conformation on hydrophobic TMS, hydrophilic FS, and a patterned TMS/FS surface. The distributions describe the probability of observing a given relative end-to-end distance, *d*. The boxes from $d = 0$ to 0.4 and from $d = 1.8$ to 2.2 represent adsorbed peptides with negligible intensity in either the acceptor or donor channel, respectively. The area of each box is proportional to the number of molecules in these extreme states. The cumulative area under the boxes and curve integrates to unity. Note that probability is reported on a logarithmic axis to highlight the minima at approximately $d = 1.14$, which are marked with a dashed vertical line. This value of d was used as a threshold to classify a given observation of peptide conformation as either "coil" ($d < 1.14$) or "helix" ($d > 1.14$). (B) Absolute end-to-end distance probability distributions (black curves) for disordered peptide based on a self-avoiding random walk in 2D and in 3D as described in the SI (eq S-2) and the end-to-end distance for the fully helical peptide (gray vertical line).

d and high d peaks were well-separated by a threshold of $d = 1.14$ so that two conformational states were readily distinguished. This general approach has previously been applied to understand the conformational states of DNA and proteins.[54,55] The only drawback to this approach was that the fraction of molecules observed in the high d state may have been increased slightly by the presence of molecules labeled with only the donor dye, but this artifact would not have changed the overall trends reported below with respect to surface chemistry and the kinetics of molecules that changed conformational state.

To assign low d and high d "states" identified by these distributions to physical molecular conformations, we carefully considered the potential conformations that an adsorbed peptide can adopt. Using NMR spectroscopy, Burkett and Read[56] found that peptides that were strongly helical in solution adopted

conformations that, when adsorbed on silica, retained significant helical character, with some helical loss at the peptide termini. Similarly, using molecular dynamics simulations, Gnanakaran[35] and co-workers characterized the conformations of a 20-residue alanine-lysine helical peptide and found that, at intermediate temperatures, in the helix−coil transition regime, helical loss was also most significant at the peptide termini. Peptides with significant helical content were considerably longer than the disordered peptides, which had an end-to-end distance distribution resembling that of a compact random coil. Thus, with respect to our experiments, while the adsorbed peptides potentially had a range of fractional helicities, the end-to-end distances were expected to be systematically larger for molecules with more helical structure. For simplicity, we refer to more-extended structures as being in the "helix" state, and to less-extended structures as being in the "coil" state throughout the rest of the paper.

If the adsorbed peptides lacked all secondary structure, then the conformation could have resembled either the structure of a disordered peptide in solution (a three-dimensional coil) or the structure of a two-dimensional "pancake," with longer end end-to-end distances.[57] Using sum frequency generation (SFG) vibrational spectroscopy to investigate adsorbed peptide conformations, Mermut and co-workers found that only certain side chains (charged, polar side chains on hydrophilic silica and alkyl side chains on hydrophobic polystyrene) had significant interactions with the surface.[58] For our alanine-lysine copeptide, it seems likely then that the coil conformations were largely three-dimensional in nature. In Figure 2B, we present theoretical distributions of the end-to-end distance for two-dimensional and three-dimensional statistical coils and for a fully helical peptide. (The details of these idealized calculations are in the Supporting Information (SI).) Fewer than 17% of the two-dimensional coils and 2% of the three-dimensional coils had end-to-end distances greater than the end-to-end distance for a fully helical peptide, as shown graphically in Figure 2B by the light and dark gray shaded areas, respectively. Thus, it seemed reasonable that helix-rich and coil states could be distinguished by end-to-end distance for the majority of expected conformations, which likely were between the extremes of being purely two-dimensional or purely three-dimensional.

Based on a long-standing model of polymer adsorption, one could also view the adsorbed peptide as a sequence of adsorbed "trains" and unbound "loops" and "tails."[59−63] An adsorbed train is a continuous section of the amino acid chain in contact with the surface, and unadsorbed segments are referred to as tails, if they are at the ends of the chain, or, loops if they are in the middle. In this picture, the end-to-end distance increases as the number and length of adsorbed trains increases, causing the adsorbed polymer to become more two-dimensional in shape. The end-to-end distance also increases when the stiffness of unbound loops increases, causing the spacing between trains to increase. In the special case of amino acid chains, helical structure would cause the stiffness of the unbound loops to increase,[64] increasing the distance between adsorbed segments.[35] Therefore, for helix-rich peptides, we would again expect the end-to-end distance to be greater than for disordered peptides, in the adsorbed state.

Identifying Distinct Regions of a Heterogeneous Surface. As discussed above, ensemble-averaged measurements have shown that peptides and proteins typically exhibit less secondary structure upon adsorption to more hydrophobic surfaces.[16,44,45,48,49] In our experiments, the measured conformations of the adsorbed peptides were very sensitive to surface chemistry. In particular, the extended helix state (identified in Figure 2A) was more strongly favored on hydrophilic FS than on hydrophobic TMS, in qualitative agreement with the previous literature on the impact of surface chemistry on helix stability.[16,42−45,48] The strong effect of surface chemistry on peptide conformation suggested that our single-molecule observations could be used to identify different surface chemistries in a heterogeneous environment based on peptide conformation.

We have adopted the approach of accumulating multivariate, single-molecule observations in spatial bins ("pixels") to construct MAPT images of surface properties. We previously used adsorption, desorption, and diffusion data to construct surface maps,[27,65] and we extended the approach here to FRET data to examine the spatial dependence of molecular conformation. Figure 3 shows MAPT images of a photopatterned surface containing circular FS holes within a TMS matrix. This patterning approach was independently validated by creating FS circles within a patterned amine-terminated organosilane monolayer to which dye molecules were covalently bound (Figure S-2). The MAPT images were assembled based on the adsorption rate and average peptide conformation in individual pixels (760 nm × 760 nm in size). The pixel size was set so that a significant number of molecules were observed in nearly all pixels (pixels with fewer than 3 observations of molecules are shaded gray in Figure 3).

Both images were assembled from the same set of ~300 000 molecular trajectories, and the spatial locations of the underlying surface chemistries were clearly distinguished via the peptide adsorption rate and average conformation. On the TMS regions (blue area), the number of adsorbed molecules (Figure 3A) was approximately 100 times greater than that on the circular FS regions (yellow area). At the boundaries between the two regions (green area), where the ozone removal of the TMS was likely incomplete, the number of adsorbed molecules was about 10 times greater than on FS. These results agreed qualitatively

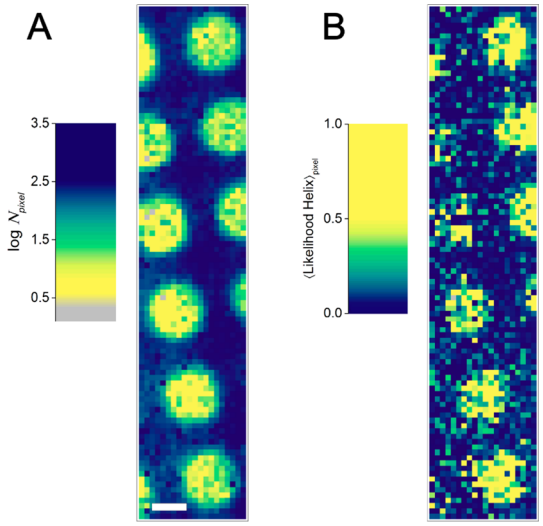

Figure 3. TMS-coated surface that was photopatterned as described in the SI, such that circular holes of FS were created in the TMS coating. (A) MAPT image showing the number of molecules that adsorbed in each pixel (N_{pixel}), which was higher on TMS than on FS regions. (B) MAPT image of the likelihood of observing peptides in the helix state in each pixel. Peptides were more commonly found in the helix state on FS than on TMS regions. The scale bar represents 5 μm. The pixel size is 760 nm $\times$ 760 nm.

with previous observations of fatty acid adsorption on TMS/FS surfaces, where more fatty acid adsorption was observed on hydrophobic TMS than on hydrophilic FS regions.[27] The difference in adsorption rates could be partially explained by viewing adsorption as a competition between the peptide adsorbate and solvent to attach to the surface.[66] Because attachment of polar solvent molecules to the surface was less favorable on hydrophobic surfaces, adsorption of the peptide was more favorable on these areas. This argument is supported by nuclear magnetic resonance relaxation spectroscopy of water molecules on silica.[67−69] Briefly, the longest orientation correlation times for water on silica surfaces (on the millisecond time scale) are thought to arise from the monolayer of water in direct contact with the solid surface.[69] This surface-bound water forms hydrogen bonds with silanol species.[19] Importantly, on an alkyl-functionalized surface, like TMS, many silanol species are reacted with the silane or rendered inaccessible to water molecules, such that water molecules are less tightly bound, forming fewer hydrogen bonds on average.[70,71] Thus, on a TMS surface, the enthalpic penalty for removing solvent-bound water is weaker, and peptides can adsorb more easily than on the FS surface. There is an electrostatic driving force for adsorption, as well, however, since positively charged lysine residues in the peptide are attracted to negatively charged silanol species on the surface.[42,43] The electrostatic driving force has an enthalpic component (Coulombic attraction) and an entropic component (counterion-release from the surface).[72,73] Intuitively, one would expect the electrostatic driving force to be greater on the more charged FS surface than on the TMS surface, and so the greater adsorption on the hydrophobic surface is primarily attributed to water-mediated effects.[74] However, biomolecule adsorption is a rich phenomenon that depends on molecular orientation and conformation, in addition to the aforementioned driving forces, and we cannot unambiguously identify the molecular basis for increased adsorption of the peptide on the more hydrophobic surface on the basis of the results reported here.

Since each spatially resolved peptide observation was classified as either helix or coil on the basis of its FRET signal, the likelihood of observing the helix state could be calculated for each pixel individually. The likelihood of observing the helix was the fraction of all observations that were helical. As shown in Figure 3B, the likelihood of observing the helix was higher overall in the circular FS regions than in the TMS regions. Compared to the spatial variation of the adsorption behavior on a given surface chemistry, the conformational behavior was more heterogeneous, both on the patterned surface (Figure 3) and on the nominally uniform control surfaces (Figures S-3 and S-4). For example, in Figure 3B, some pixels (blue, green) in the circular FS regions had fewer observations of helical peptides than the more typical pixels (yellow), whereas FS regions in the adsorption maps (Figure 3A) were much more uniform. Therefore, for purposes of comparing the different surfaces chemistries, we used the more homogeneous adsorption MAPT image (Figure 3A) to select regions for comparison to unpatterned (control) FS and TMS surfaces. Qualitatively, regions of low, intermediate, and high adsorption were distinguished in Figure 3A, corresponding to regions with hydrophilic, intermediate, and hydrophobic surface chemistry. We constructed a probability distribution of the number of adsorption events per pixel (Figure 4A) and used this distribution to set thresholds for distinguishing these different surface regions of low, medium, and high adsorption rate.

For each of these regions with different adsorption rates, we calculated the likelihood of observing the helical state, and compared the identified regions of the patterned surface to the control TMS and FS surfaces (Figure 4B). We found that the conformations on the high adsorption regions were statistically similar to the control TMS surface and that the low adsorption regions were similar to the control FS surface. These results demonstrated that statistically meaningful comparisons could be made of molecular conformations on microscopic regions of a heterogeneous surface using the MAPT technique. This validation of the MAPT approach also suggested that the heterogeneity in conformational behavior seen in the circular FS regions of the photopatterned surface and also seen on the control FS surface (Figure S-4) resulted from

meaningful differences in surface chemistry, as opposed to having been a statistical artifact.

Contributions of Adsorption/Desorption and Folding/Unfolding Processes to Average Conformation. The difference in conformation (likelihood of the helix state) on the FS and TMS surfaces could potentially have resulted from a number of different physical mechanisms.

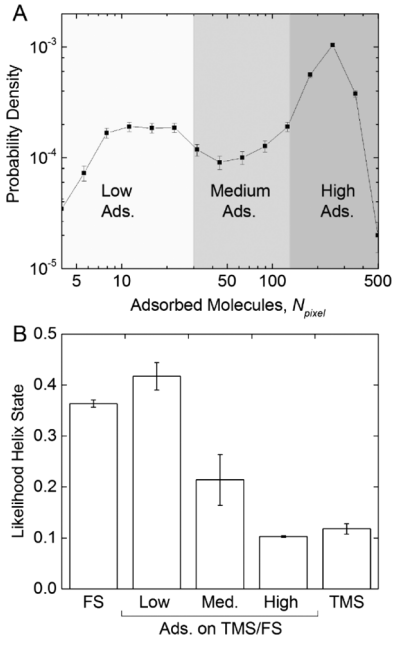

Figure 4. (A) Probability distribution of the number of adsorbed molecules per pixel (N_{pixel}) on a patterned TMS/FS surface. The shading indicates subsets of data selected for subsequent analysis corresponding to regions of low, medium, and high adsorption (appearing as yellow, green, and blue in Figure 3A), which cover 26%, 16%, and 58% of the total surface area, respectively. The low and high adsorption regions were patterned regions of FS and TMS, respectively. The medium adsorption regions were located at the interface between the TMS and FS regions. (B) Likelihood of observing peptides in the helix state on control FS and TMS surfaces and in the regions of the patterned TMS/FS surface with low, medium, and high adsorption. Error bars denote standard error of the mean.

For example, single-molecule imaging of an adsorbed enzyme, organophosphorus hydrolase, revealed that most proteins that adsorbed in the folded state quickly unfolded prior to desorption.[55] Thus, the initial conformation (measured immediately after adsorption) favored the folded state when compared to the final conformation (measured in the frame prior to desorption). We performed a similar analysis here, comparing the likelihood of observing the helix state immediately after adsorption and immediately prior to desorption (Figure 5A). Interestingly, we did not see significant differences between the initial and final conformations of peptides adsorbed to either the TMS or FS surface (Figure 5A). This implied that most peptides remained in the same conformation in which they adsorbed or relaxed to the most favorable conformational state within 100 ms (one frame time) of adsorbing to the surface and then remained in a stable conformation. The prevalence of unfolding processes probably depends on how exactly the molecules become immobilized on the surface. We compared our current results on surface-induced unfolding with peptides to the previous results with proteins.[55] For a protein, there were many points of potential surface attachment, and the immobilization of a relatively small part of the structure on the surface might not have greatly diminished the ability of the molecule to unfold. For a smaller peptide, the points of attachment were much more limited, and the adsorbed peptide may have been pinned on the surface so that it could rarely change conformational state without desorbing.

The average conformational state was not noticeably affected by folding/unfolding processes, which were rare, but it could have been affected by conformation-dependent desorption kinetics, for example, if coil peptides had longer surface residence times than helix peptides. We did not, however, find a significant difference between the average desorption rate constants for molecules that adsorbed in the helix state

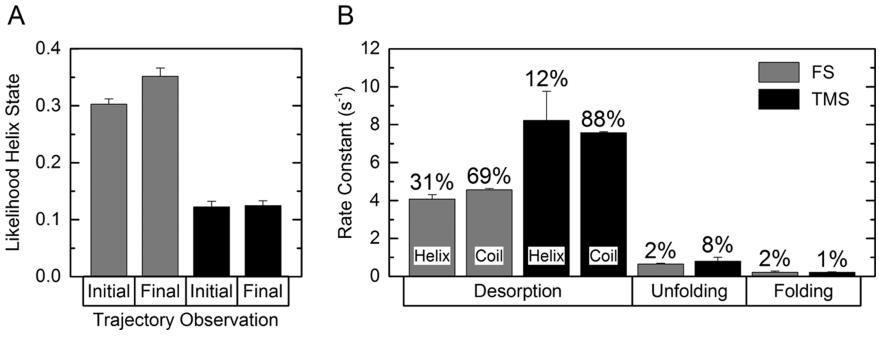

Figure 5. (A) Likelihood of observing the helix state in the "initial" observation for a given trajectory (i.e., the first image after adsorption) and in the "final" observation (i.e., the last image prior to desorption). (B) Mean rate constants of desorption, unfolding from the helix to coil state, and folding from the coil to helix state. Mean rate constants were obtained by fitting the distributions of surface residence times (desorption rate), initial helix states (unfolding rate), and initial coil states (folding rate) as shown in Figure S-5 with mixtures of exponential distributions (eq 2). The desorption rate constants were calculated separately for molecules initially in the helix state and the coil state, as labeled on the bars. The percentage of molecules undergoing each process is given above the applicable bar. Error bars represent standard error of three different subsets of the data.

versus the coil state on either TMS or FS (Figure 5B). So the higher likelihood of observing the helix state on FS than on TMS could not be attributed to a large difference in average surface residence times of different conformations. Having eliminated the effects of folding and desorption processes, we therefore concluded that the average conformational state was mostly determined by a bias in the initial conformation adopted upon adsorption. In other words, the difference in adsorption rates of the helix and coil peptides determined the average surface conformation, and these adsorption rates had a strong dependence on the surface hydrophobicity. We cannot discern to what extent fast submillisecond relaxation processes of the adsorbed peptide contributed to these observations, but the conformations were relatively stable. Most of the molecules (~90%) desorbed without changing conformation and followed approximately the same average desorption kinetics regardless of conformation.

Heterogeneous Peptide Behavior on Nominally Uniform Surfaces. The unique advantage of the single-molecule approach is access to the full distribution of molecular behaviors, which can give insight into the effects of fine spatial differences on nominally uniform surfaces. Surface residence time distributions are especially sensitive to surface heterogeneity, and the presence of distinctly different types of surface sites can lead to broadly distributed residence times.[75−77] Therefore, to assess the chemical heterogeneity of nominally uniform surfaces, we fit the surface residence time distribution to mixture models, as described in the Methods section, and examined the populations of surface residence times. While residence time distributions on both TMS and FS surfaces required three populations for an accurate fit, the fraction of molecules exhibiting anomalously long residence times (*i.e.*, belonging to the two longer-lived populations) was ~10% on TMS and greater than 20% on FS (Table S-1). This agreed with our initial assessment, based on visual inspection of the maps of adsorption and conformation, that FS might be intrinsically more heterogeneous than TMS. Interestingly, the increased presence of long-lived species on FS compared to TMS is supported by previous atomic force microscopy (AFM) measurements.[8] Adsorbed DNA could be observed directly on FS, but remained AFM-invisible on TMS due to fast desorption kinetics. While AFM is undeniably a powerful tool, in an actual molecular device, all species present will contribute to overall performance; clearly, single-molecule imaging can supplement characterization techniques, such as AFM, that are sensitive to different time scales.

Surface heterogeneity will have an important effect on surface-based assembly if it alters the spatial distribution of adsorbed, *functional* building block materials (*e.g.*, peptides in the helical state rather than the disordered coil state). While the residence time

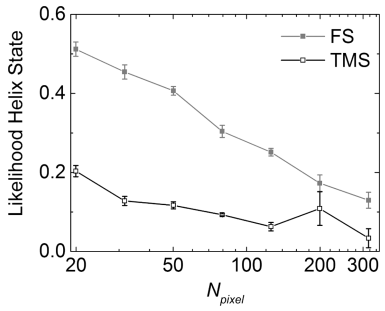

Figure 6. Likelihood of helical peptide conformation for observations in adsorption map pixels with N_{pixel} adsorption events. Equivalent surface maps of adsorption were constructed for both surfaces with an average N_{pixel} of 52. Error bars denote standard error.

distributions suggested that the uniform surfaces were chemically heterogeneous, mapping the surface quantified the length scale of that heterogeneity. In this work, we validated our mapping technique using the patterned TMS/FS surface and showed that adsorption rates and conformational states were sensitive to variations in surface chemistry over microscopic length scales. This approach could be applied with confidence to quantify heterogeneity on the nominally uniform TMS and FS surfaces and to examine the mechanistic effects of surface heterogeneity. To determine if the heterogeneity in the adsorption and conformational behavior was correlated, we calculated the likelihood of the helix state in surface map pixels with different numbers of adsorption events (Figure 6). Interestingly, we found that helical conformations were more likely to be observed than coil conformations on regions with weaker adsorption (lower values of N_{pixel}) on both TMS and FS. We observed a stronger correlation between adsorption rate and conformational state on FS than on TMS, suggesting that FS was less chemically uniform. The chemical heterogeneity of FS might have been due the presence of silanol groups with different characteristic acidities (e.g., isolated, vicinal, or germinal silanols), and this would have affected the behavior of adsorbate molecules because more acidic silanols form stronger hydrogen bonds.[19,78] It is worth noting that this type of chemical heterogeneity often accompanies physical heterogeneity (*i.e.*, topographic features like pits and scratches); on crystalline silica surfaces, different crystal planes are "cut" at these topographic defects, resulting in different characteristic silanol species at the surface.[19] In agreement with this picture, strong adsorption of polar molecules is often correlated with topographic features at the nanoscale, as combined atomic force microscopy and fluorescence imaging have shown.[79] In our system, the TMS coating of FS had the effect of introducing hydrophobic ligands, which capped many of the diverse silanol species. Nevertheless, the same phenomena of helical conformations being more favorable on regions with weaker adsorption was observed on TMS and FS. So while

"passivating" layers such as TMS can help reduce spatial heterogeneity, the effect of spatial heterogeneity on conformation and adsorption of macromolecule seems to be quite general in nature.

CONCLUSIONS

Using a helical peptide and surfaces with varying hydrophobicity, we have demonstrated the ability to correlate molecular conformation with microscopic regions of a surface. Extended peptide conformations, likely more helical in nature, were more favorable on hydrophilic FS than on hydrophobic TMS at the single-molecule level on patterned surfaces and on uniform control surfaces. The FS surface captured more molecules in the helix state than did TMS, and these conformational states were stable, such that most peptides did not undergo a conformational change prior to desorption from the surface. In other words, the affinities of the helix and coil conformations for the different surfaces dictated their average folded state, as opposed to surface-induced unfolding being the primary effect. On FS, extremely long surface residence times were observed relatively often; these rare molecular populations could dominate measurements made over longer time scales and were indirect evidence of the heterogeneity of the surface. Quantifying the observations made on the surface maps revealed that the helical conformation was more favorable on regions with low adsorption rates. These types of local variations in surface chemistry could strongly affect the ability of adsorbed biomolecules to recognize other biomolecules through specific interactions and cold be important in determining the final structure of self-assembled materials or devices. This type of analysis should prove valuable in characterizing surface coatings designed to promote biomolecular recognition not only for the assembly of molecular building blocks but also for surface-based sensors. Typically, the primary role of the coating is to control adsorption phenomena, but surface-induced denaturation of the molecular building blocks or analytes of interest is clearly undesirable and seemingly correlated with the adsorption kinetics on the surface. Spatial heterogeneity is an important feature of such coatings, and we have provided a new, rigorous method for fine spatial characterization of surface chemistry. This work demonstrates the importance of considering spatial heterogeneity at microscopic length-scales when interpreting ensemble-averaged experiments and especially when making comparisons to molecular simulations. With this technique in hand, we can harness the unique capabilities of single-molecule imaging for characterizing molecular conformation in diverse biological and functional materials systems.

METHODS

Solutions of End-Labeled Peptide. A fluorescently labeled peptide (purity > 95% by reversed phase high performance liquid chromatography) was purchased from Anaspec (Fremont, CA). The amino acid sequence was AAAKAAKAKAAKAAAAKAAK-KAAAAKAK, with an amidated C-terminus, HiLyte Fluor 488 conjugated to the N-terminus and HiLyte Fluor 594 conjugated to the side chain of the C-terminal lysine. For single-molecule imaging experiments, the peptide was dissolved in phosphate buffered saline (Gibco, calcium and magnesium free, pH 7.4, ionic strength 162 mM, Debye length 0.8 nm) to 10^{-9}–10^{-11} M. Prior to acquiring images, the solution concentration was increased until the field of view had sufficient densities of adsorbed molecules to provide robust statistics ($\sim 10^{-3}$ molecules μm^{-2}).

Surface Preparation and Characterization. Two inch diameter fused silica (FS) wafers (Mark Optics) were washed with detergent (Micro 90, International Product Corp) and thoroughly rinsed with ultrapure water with 18 MΩ cm resistivity (Milli-Q UV Plus, EMD Millipore). Wafers were immediately immersed in a 70% sulfuric acid, 30% hydrogen peroxide, piranha solution (warning: hazardous corrosive, strongly oxidizing solution) for 1 h, rinsed with ultrapure water, dried with nitrogen, and further cleaned in a UV/ozone cleaner (Novascan) for 1 h, as previously described.[80] The cleaned wafers were then used for experiments with uniform FS. To create a trimethylsilyl (TMS) monolayer, the cleaned wafers were placed in the lid of a sealed, 2 in. diameter jar with 5 mL of hexamethyldisilazane in the bottom, for 18 h at room temperature. After this deposition, the TMS water contact angle was measured with a custom-built goniometer, using an ~1 μL sessile drop on three different positions on the wafer.[81] Using a contact photomask and an ultraviolet light source, the TMS was patterned as described in the SI to create a TMS/FS patterned surface.

Single-Molecule Total Internal Reflection Fluorescence Microscopy (TIRFM). Our TIRF microscope has been described in detail elsewhere.[82,83] Briefly, it consisted of an inverted Nikon TE-2000 microscope with 60× objective with 1.5× auxiliary magnification, prism-based illumination provided by a 491 nm laser, flow cell, an Optosplit III Image Splitter (Cairn Research) and an electron multiplied CCD-camera (Andor). The microscope was focused at the interface between the surface of interest and a stagnant peptide solution, which was held at room temperature. The image was split by a 580 nm dichroic mirror (Chroma) into donor and acceptor channels, which were each projected onto different regions of the CCD sensor. The donor channel was filtered with a bandpass filter with a 95% transmission interval, centered at 525 nm, with a width of 39 nm (Semrock), and the acceptor channel was filtered with a 591 nm long-pass filter (Semrock). The channels were aligned and molecules identified as described previously (using an image processing routine where the raw images were convolved with a disk matrix and then thresholded to identify distinct objects).[76,83] Only molecules adsorbed to the interface were localized during image processing because diffusion in solution was too fast to allow localization at the 100 ms frame acquisition times used in these experiments. Previous studies of FS and TMS surfaces have shown that adsorbed molecules are typically confined to regions smaller than the localization precision (~100 nm).[65,84] Molecular trajectories were formed by tracking the closest objects in sequential frames that were less than 445 nm (3 pixels) apart. (The finite tracking radius accounted for uncertainty in the channel alignment and object localization.) All image processing and object tracking was performed in Mathematica 9 (Wolfram).

Quantification of Förster Resonance Energy Transfer (FRET). FRET is the nonradiative transfer of energy from a donor to acceptor fluorophore across a distance r with an efficiency that is proportional to r^{-6} and equals 50% at the Förster radius (R_o).[28]

For the HiLyte Fluor 488/594 dye pair, we calculated R_o to be 5.1 nm using standard Förster theory (assuming unhindered dye rotation, orientation factor of 2/3) and the published absorption and emission spectra.[85] The absolute donor−acceptor distance is given by

$$r = \mu d = \mu(F_D/F_A)^{1/6} \quad (1)$$

where F_D is the fluorescence intensity of the molecule in the donor channel and F_A is the fluorescence intensity in the acceptor channel. The factor $\mu = R_o[(F_A|_{r\to 0})/(F_D|_{r\to\infty})]$ depends on the Förster radius and the fluorescence intensities of the donor and acceptor at known separation distances. While the donor fluorescence in the absence of acceptor, $F_D|_{r\to\infty}$, can be empirically measured, the fluorescence of the acceptor in the limit of 100% efficient energy transfer, $F_A|_{r\to 0}$, can be derived only by fixing the dyes with subnanometer precision and assuming no donor quenching by non-FRET collisional processes. The efficiency of the resonance energy transfer may also be strongly affected by the presence of the solid surface, which can hinder dye rotation or interact with the dyes electronically. The absolute values of F_A may also have been slightly increased by bleeding of the donor emission into the acceptor channel; however, this bleed-through effect was found to be minor for spectrally similar donor and acceptor dyes.[86] Due to the significant uncertainty in the parameter μ and the absolute fluorescence intensities, we reported our data using the relative end-to-end distance $d = r/\mu = (F_D/F_A)^{1/6}$ as in previous single-molecule FRET studies of freely adsorbing molecules.[54,55,83,87]

Calculation of Likelihood of Conformational States. For a data set with N total observations, the likelihood of observing a helix is n(helix)/N, where n(helix) is the number of observations of the helix state. For the MAPT images (e.g., Figure 3B), we used the notation $\langle\text{Likelihood Helix}\rangle_{\text{pixel}}$ to denote that the likelihood was calculated for observations in each pixel separately. For all other calculations, the data was pooled from either the whole image or pixels with a specific number of adsorption events or from trajectories with specific surface residence times. When comparing the initial and final observations in a trajectory, only trajectories at least 0.2 s (two frames) long were considered.

Characterization of Desorption and Folding/Unfolding Kinetics. For each molecule, the time interval between adsorption and desorption was recorded as the surface residence time t. For each data set considered, we compiled a complementary cumulative distribution $F(t)$ of residence times. We fit these distributions using an exponential mixture model, where each component distribution represents a distinct first-order kinetic pathway.[88]

$$F(\tau) = \sum_{i=1}^{n} p_i e^{-t/\tau_i} \quad (2)$$

Each component distribution of the mixture model had a characteristic residence time τ_i and represented a fraction p_i of the molecules. The distribution was constrained so that $\Sigma p_i = 1$ For a more detailed discussion of the significance of the model and fitting procedure, see Mabry et al.[76] We fit the distributions using the minimum number of components necessary for good fits ($R^2 > 0.99$) to find the average surface residence time, given by $\langle\tau\rangle = \Sigma p_i\tau_i$. The desorption rate constant was given by $\langle\tau\rangle^{-1}$. To characterize the folding and unfolding kinetics, we measured the initial state residence time of the coil and helix conformational states, respectively. We ignored subsequent conformational changes because the probability of observing a subsequent conformational change depends on the length of the trajectory and the previous state residence times, such that the data could not easily be normalized.[54] We utilized a previously outlined strategy to construct probability distributions of initial state residence times (eq S-5), which were corrected for observation bias (the bias to only observe state residence times shorter than the surface residence times).[54] We fit the initial state residence time distributions to a mixture of exponential distributions in the same manner as the surface residence times and reported the average rate constants derived from these fits. To decrease the effect of anomalously bright, one-frame "noise" objects, we included only surface residence times and initial conformational state times that were 0.2 s or longer. The percentages of molecules undergoing the associated processes of desorption and folding/unfolding were calculated based on the subset of trajectories that could possibly exhibit these phenomena (specifically 0.2 s or longer in the case of desorption and 0.3 s or longer in the case of folding/unfolding).

Conflict of Interest: The authors declare no competing financial interest.

Acknowledgment. The authors thank B. B. Langdon for careful editing of the manuscript. The authors acknowledge primary support from the U.S. Department of Energy Basic Energy Sciences, Chemical Sciences, Geosciences, and Biosciences Division (DE-SC0001854) for all aspects of the research reported here, including instrumentation, salary and stipend support, materials/supplies, *etc.* J.N.M was partially supported by a U.S. Department of Education Graduate Assistance in Areas of National Need Fellowship (P200A120125). Stipend support for M.K. and partial materials cost were paid by NIH Fellowship 5F32GM091777-02. This work utilized the Janus supercomputer, which is supported by the National Science Foundation (award number CNS-0821794) and the University of Colorado Boulder. The Janus supercomputer is a joint effort of the University of Colorado Boulder, the University of Colorado Denver, and the National Center for Atmospheric Research. Data storage resources were provided by NSF-MRI Grant ACI-1126839, MRI: Acquisition of a Scalable Petascale Storage Infrastructure for Data-Collections and Data-Intensive Discovery.

Supporting Information Available: Characterization of the peptide structure and surface patterning technique, maps of the uniform control surfaces, and detailed data on kinetic processes and photophysical effects. The Supporting Information is available free of charge on the ACS Publications website at DOI: 10.1021/acsnano.5b02071.

REFERENCES AND NOTES

1. Maune, H. T.; Han, S.; Barish, R. D.; Bockrath, M.; Goddard, W. A.; Rothemund, P. W. K.; Winfree, E. Self-Assembly of Carbon Nanotubes into Two-Dimensional Geometries Using DNA Origami Templates. *Nat. Nanotechnol.* **2010**, *5*, 61–66.
2. Kuzyk, A.; Schreiber, R.; Fan, Z.; Pardatscher, G.; Roller, E.-M.; Hogele, A.; Simmel, F. C.; Govorov, A. O.; Liedl, T. DNA-Based Self-Assembly of Chiral Plasmonic Nanostructures with Tailored Optical Response. *Nature* **2012**, *483*, 311–314.
3. Hyman, P.; Valluzzi, R.; Goldberg, E. Design of Protein Struts for Self-Assembling Nanoconstructs. *Proc. Natl. Acad. Sci. U. S. A.* **2002**, *99*, 8488–8493.
4. Park, S. Y.; Lytton-Jean, K. R. A.; Lee, B.; Weigand, S.; Schatz, G. C.; Mirkin, C. A. DNA Programmable Nanoparticle Crystallization. *Nature* **2008**, *451*, 553–556.
5. Jones, M. R.; Macfarlane, R. J.; Lee, B.; Zhang, J. A.; Young, K. L.; Senesi, A. J.; Mirkin, C. A. DNA-Nanoparticle Superlattices Formed from Anisotropic Building Blocks. *Nat. Mater.* **2010**, *9*, 913–917.
6. Merzlyak, A.; Lee, S.-W. Phage as Templates for Hybrid Materials and Mediators for Nanomaterial Synthesis. *Curr. Opin. Chem. Biol.* **2006**, *10*, 246–252.
7. Oshea, E. K.; Rutkowski, R.; Kim, P. S. Evidence That the Leucine Zipper Is a Coiled Coil. *Science* **1989**, *243*, 538–542.
8. Gopinath, A.; Rothemund, P. W. K. Optimized Assembly and Covalent Coupling of Single-Molecule DNA Origami Nanoarrays. *ACS Nano* **2014**, *8*, 12030–12040.
9. Nuraje, N.; Banerjee, I. A.; MacCuspie, R. I.; Yu, L. T.; Matsui, H. Biological Bottom-up Assembly of Antibody Nanotubes on Patterned Antigen Arrays. *J. Am. Chem. Soc.* **2004**, *126*, 8088–8089.
10. Heller, M. J. DNA Microarray Technology: Devices, Systems, and Applications. *Annu. Rev. Biomed. Eng.* **2002**, *4*, 129–153.
11. Cretich, M.; Damin, F.; Pirri, G.; Chiari, M. Protein and Peptide Arrays: Recent Trends and New Directions. *Biomol. Eng.* **2006**, *23*, 77–88.

12. Jamadagni, S. N.; Godawat, R.; Dordick, J. S.; Garde, S. How Interfaces Affect Hydrophobically Driven Polymer Folding. *J. Phys. Chem. B* **2009**, *113*, 4093–4101.
13. Claesson, P. M.; Blomberg, E.; Froberg, J. C.; Nylander, T.; Arnebrant, T. Protein Interactions at Solid-Surfaces. *Adv. Colloid Interface Sci.* **1995**, *57*, 161–227.
14. Raffaini, G.; Ganazzoli, F. Protein Adsorption on Biomaterial and Nanomaterial Surfaces: A Molecular Modeling Approach to Study Non-Covalent Interactions. *J. Appl. Biomater. Biomech.* **2010**, *8*, 135–145.
15. Jones, R. A. L.; Richards, R. W. *Polymers at Surfaces and Interfaces*; Cambridge University Press: Cambridge, 1999.
16. Balamurugan, K.; Gopalakrishnan, R.; Raman, S. S.; Subramanian, V. Exploring the Changes in the Structure of A-Helical Peptides Adsorbed onto a Single Walled Carbon Nanotube Using Classical Molecular Dynamics Simulation. *J. Phys. Chem. B* **2010**, *114*, 14048–14058.
17. Gong, P.; Levicky, R. DNA Surface Hybridization Regimes. *Proc. Natl. Acad. Sci. U. S. A.* **2008**, *105*, 5301–5306.
18. Rafferty, J. L.; Siepmann, J. I.; Schure, M. R. Influence of Bonded-Phase Coverage in Reversed-Phase Liquid Chromatography *via* Molecular Simulation. II. Effects on Solute Retention. *J. Chromatogr. A* **2008**, *1204*, 20–27.
19. Rimola, A.; Costa, D.; Sodupe, M.; Lambert, J.-F.; Ugliengo, P. Silica Surface Features and Their Role in the Adsorption of Biomolecules: Computational Modeling and Experiments. *Chem. Rev.* **2013**, *113*, 4216–4313.
20. Doshi, D. A.; Watkins, E. B.; Israelachvili, J. N.; Majewski, J. Reduced Water Density at Hydrophobic Surfaces: Effect of Dissolved Gases. *Proc. Natl. Acad. Sci. U. S. A.* **2005**, *102*, 9458–9462.
21. Scatena, L. F.; Brown, M. G.; Richmond, G. L. Water at Hydrophobic Surfaces: Weak Hydrogen Bonding and Strong Orientation Effects. *Science* **2001**, *292*, 908–912.
22. Patel, A. J.; Varilly, P.; Chandler, D.; Garde, S. Quantifying Density Fluctuations in Volumes of All Shapes and Sizes Using Indirect Umbrella Sampling. *J. Stat. Phys.* **2011**, *145*, 265–275.
23. Mrksich, M.; Whitesides, G. M. Using Self-Assembled Monolayers to Understand the Interactions of Man-Made Surfaces with Proteins and Cells. *Annu. Rev. Biophys. Biomol. Struct.* **1996**, *25*, 55–78.
24. Ramos, R.; Gordon, M. J. Reflection-Mode, Confocal, Tip-Enhanced Raman Spectroscopy System for Scanning Chemical Microscopy of Surfaces. *Rev. Sci. Instrum.* **2012**, *83*, -.
25. Mazzola, L. T.; Frank, C. W.; Fodor, S. P.; Mosher, C.; Lartius, R.; Henderson, E. Discrimination of DNA Hybridization Using Chemical Force Microscopy. *Biophys. J.* **1999**, *76*, 2922–2933.
26. Woo, S.; Rothemund, P. W. K. Self-Assembly of Two-Dimensional DNA Origami Lattices Using Cation-Controlled Surface Diffusion. *Nat. Commun.* **2014**, *5*, 4889.
27. Walder, R.; Nelson, N.; Schwartz, D. K. Super-Resolution Surface Mapping Using the Trajectories of Molecular Probes. *Nat. Commun.* **2011**, 2.
28. Lakowicz, J. R. Energy Transfer. In *Principles of Fluorescence Spectroscopy*, 3rd ed.; Lakowicz, J., Ed.; Springer: New York, 2006; pp 443−475.
29. Huang, Y.; Duan, X.; Wei, Q.; Lieber, C. M. Directed Assembly of One-Dimensional Nanostructures into Functional Networks. *Science* **2001**, *291*, 630–633.
30. Penzo, E.; Wang, R.; Palma, M.; Wind, S. J. Selective Placement of DNA Origami on Substrates Patterned by Nanoimprint Lithography. *J. Vac. Sci. Technol. B* **2011**, *29*, 06F205.
31. Marqusee, S.; Robbins, V. H.; Baldwin, R. L. Unusually Stable Helix Formation in Short Alanine-Based Peptides. *Proc. Natl. Acad. Sci. U. S. A.* **1989**, *86*, 5286–5290.
32. Scholtz, J. M.; Baldwin, R. L. The Mechanism of Alpha-Helix Formation by Peptides. *Annu. Rev. Biophys. Biomol. Struct.* **1992**, *21*, 95–118.
33. Jas, G. S.; Hegefeld, W. A.; Middaugh, C. R.; Johnson, C. K.; Kuczera, K. Detailed Microscopic Unfolding Pathways of an Alpha-Helix and a Beta-Hairpin: Direct Observation and Molecular Dynamics. *J. Phys. Chem. B* **2014**, *118*, 7233–7246.
34. Zagrovic, B.; Jayachandran, G.; Millett, I. S.; Doniach, S.; Pande, V. S. How Large Is an Alpha-Helix? Studies of the Radii of Gyration of Helical Peptides by Small-Angle X-Ray Scattering and Molecular Dynamics. *J. Mol. Biol.* **2005**, *353*, 232–241.
35. Gnanakaran, S.; Hochstrasser, R. M.; Garcia, A. E. Nature of Structural Inhomogeneities on Folding a Helix and Their Influence on Spectral Measurements. *Proc. Natl. Acad. Sci. U. S. A.* **2004**, *101*, 9229–9234.
36. Thompson, P. A.; Munoz, V.; Jas, G. S.; Henry, E. R.; Eaton, W. A.; Hofrichter, J. The Helix-Coil Kinetics of a Heteropeptide. *J. Phys. Chem. B* **2000**, *104*, 378–389.
37. Wang, T.; Zhu, Y.; Getahun, Z.; Du, D.; Huang, C. Y.; Degrado, W. F.; Gai, F. Length Dependent Helix-Coil Transition Kinetics of Nine Alanine-Based Peptides. *J. Phys. Chem. B* **2004**, *108*, 15301–15310.
38. Sorin, E. J.; Pande, V. S. Exploring the Helix-Coil Transition *via* All-Atom Equilibrium Ensemble Simulations. *Biophys. J.* **2005**, *88*, 2472–2493.
39. Nymeyer, H.; Garcia, A. E. Simulation of the Folding Equilibrium of Alpha-Helical Peptides: A Comparison of the Generalized Born Approximation with Explicit Solvent. *Proc. Natl. Acad. Sci. U. S. A.* **2003**, *100*, 13934–13939.
40. Chakrabartty, A.; Kortemme, T.; Baldwin, R. L. Helix Propensities of the Amino-Acids Measured in Alanine-Based Peptides without Helix-Stabilizing Side-Chain Interactions. *Protein Sci.* **1994**, *3*, 843–852.
41. Doig, A. J.; Chakrabartty, A.; Klingler, T. M.; Baldwin, R. L. Determination of Free Energies of N-Capping in α-Helixes by Modification of the Lifson-Roig Helix-Coil Theory to Include N- and C-Capping. *Biochemistry* **1994**, *33*, 3396–3403.
42. Lundqvist, M.; Nygren, P.; Jonsson, B. H.; Broo, K. Induction of Structure and Function in a Designed Peptide Upon Adsorption on a Silica Nanoparticle. *Angew. Chem., Int. Ed.* **2006**, *45*, 8169–8173.
43. Nygren, P.; Lundqvist, M.; Broo, K.; Jonsson, B. H. Fundamental Design Principles That Guide Induction of Helix Upon Formation of Stable Peptide-Nanoparticle Complexes. *Nano Lett.* **2008**, *8*, 1844–1852.
44. Zhao, X.; Liu, R.; Chi, Z.; Teng, Y.; Qin, P. New Insights into the Behavior of Bovine Serum Albumin Adsorbed onto Carbon Nanotubes: Comprehensive Spectroscopic Studies. *J. Phys. Chem. B* **2010**, *114*, 5625–5631.
45. Matsuura, K.; Saito, T.; Okazaki, T.; Ohshima, S.; Yumura, M.; Iijima, S. Selectivity of Water-Soluble Proteins in Single-Walled Carbon Nanotube Dispersions. *Chem. Phys. Lett.* **2006**, *429*, 497–502.
46. Wang, S.; Humphreys, E. S.; Chung, S.-Y.; Delduco, D. F.; Lustig, S. R.; Wang, H.; Parker, K. N.; Rizzo, N. W.; Subramoney, S.; Chiang, Y.-M.; Jagota, A. Peptides with Selective Affinity for Carbon Nanotubes. *Nat. Mater.* **2003**, *2*, 196–200.
47. Dieckmann, G. R.; Dalton, A. B.; Johnson, P. A.; Razal, J.; Chen, J.; Giordano, G. M.; Muñoz, E.; Musselman, I. H.; Baughman, R. H.; Draper, R. K. Controlled Assembly of Carbon Nanotubes by Designed Amphiphilic Peptide Helices. *J. Am. Chem. Soc.* **2003**, *125*, 1770–1777.
48. Roach, P.; Farrar, D.; Perry, C. C. Interpretation of Protein Adsorption: Surface-Induced Conformational Changes. *J. Am. Chem. Soc.* **2005**, *127*, 8168–8173.
49. Lu, D. R.; Park, K. Effect of Surface Hydrophobicity on the Conformational-Changes of Adsorbed Fibrinogen. *J. Colloid Interface Sci.* **1991**, *144*, 271–281.
50. Wannerberger, K.; WelinKlintstrom, S.; Arnebrant, T. Activity and Adsorption of Lipase from Humicola Lanuginosa on Surfaces with Different Wettabilities. *Langmuir* **1997**, *13*, 784–790.
51. Halthur, T. J.; Arnebrant, T.; Macakova, L.; Feiler, A. Sequential Adsorption of Bovine Mucin and Lactoperoxidase to Various Substrates Studied with Quartz Crystal Microbalance with Dissipation. *Langmuir* **2010**, *26*, 4901–4908.
52. Wannerberger, K.; Arnebrant, T. Adsorption of Lipase to Silica and Methylated Silica Surfaces. *J. Colloid Interface Sci.* **1996**, *177*, 316–324.

53. Sotres, J.; Madsen, J. B.; Arnebrant, T.; Lee, S. Adsorption and Nanowear Properties of Bovine Submaxillary Mucin Films on Solid Surfaces: Influence of Solution Ph and Substrate Hydrophobicity. *J. Colloid Interface Sci.* **2014**, *428*, 242–250.
54. Kastantin, M.; Schwartz, D. K. DNA Hairpin Stabilization on a Hydrophobic Surface. *Small* **2013**, *9*, 933–941.
55. McLoughlin, S. Y.; Kastantin, M.; Schwartz, D. K.; Kaar, J. L. Single-Molecule Resolution of Protein Structure and Interfacial Dynamics on Biomaterial Surfaces. *Proc. Natl. Acad. Sci. U. S. A.* **2013**, *110*, 19396–19401.
56. Burkett, S. L.; Read, M. J. Adsorption-Induced Conformational Changes of A-Helical Peptides. *Langmuir* **2001**, *17*, 5059–5065.
57. Sukhishvili, S. A.; Chen, Y.; Muller, J. D.; Gratton, E.; Schweizer, K. S.; Granick, S. Surface Diffusion of Poly-(ethylene glycol). *Macromolecules* **2002**, *35*, 1776–1784.
58. Mermut, O.; Phillips, D. C.; York, R. L.; McCrea, K. R.; Ward, R. S.; Somorjai, G. A. *In situ* Adsorption Studies of a 14-Amino Acid Leucine-Lysine Peptide onto Hydrophobic Polystyrene and Hydrophilic Silica Surfaces Using Quartz Crystal Microbalance, Atomic Force Microscopy, and Sum Frequency Generation Vibrational Spectroscopy. *J. Am. Chem. Soc.* **2006**, *128*, 3598–3607.
59. Lai, P. Y. Statics and Dynamics of a Polymer-Chain Adsorbed on a Surface - Monte-Carlo Simulation Using the Bond-Fluctuation Model. *Phys. Rev. E Stat. Nonlin. Soft Matter Phys.* **1994**, *49*, 5420–5430.
60. Eisenriegler, E.; Kremer, K.; Binder, K. Adsorption of Polymer Chains at Surfaces: Scaling and Monte Carlo Analyses. *J. Chem. Phys.* **1982**, *77*, 6296–6320.
61. Skaug, M. J.; Mabry, J. N.; Schwartz, D. K. Single-Molecule Tracking of Polymer Surface Diffusion. *J. Am. Chem. Soc.* **2014**, *136*, 1327–1332.
62. Sukhishvili, S. A.; Chen, Y.; Muller, J. D.; Gratton, E.; Schweizer, K. S.; Granick, S. Diffusion of a Polymer "Pancake". *Nature* **2000**, *406*, 146–146.
63. Wong, J. S. S.; Hong, L.; Bae, S. C.; Granick, S. Polymer Surface Diffusion in the Dilute Limit. *Macromolecules* **2011**, *44*, 3073–3076.
64. Kageshima, M.; Lantz, M. A.; Jarvis, S. P.; Tokumoto, H.; Takeda, S.; Ptak, A.; Nakamura, C.; Miyake, J. Insight into Conformational Changes of a Single A-Helix Peptide Molecule through Stiffness Measurements. *Chem. Phys. Lett.* **2001**, *343*, 77–82.
65. Skaug, M. J.; Schwartz, D. K. Using the Dynamics of Fluorescent Cations to Probe and Map Charged Surfaces. *Soft Matter* **2012**, *8*, 12017–12024.
66. Honciuc, A.; Baptiste, D. J.; Campbell, I. P.; Schwartz, D. K. Solvent Dependence of the Activation Energy of Attachment Determined by Single Molecule Observations of Surfactant Adsorption. *Langmuir* **2009**, *25*, 7389–7392.
67. Stapf, S.; Kimmich, R.; Niess, J. Microstructure of Porous Media and Field-Cycling Nuclear Magnetic Relaxation Spectroscopy. *J. Appl. Phys.* **1994**, *75*, 529–537.
68. Stapf, S.; Kimmich, R.; Seitter, R. O. Proton and Deuteron Field-Cycling Nmr Relaxometry of Liquids in Porous Glasses: Evidence for Levy-Walk Statistics. *Phys. Rev. Lett.* **1995**, *75*, 2855–2858.
69. Zimmerman, J. R.; Brittin, W. E. Nuclear Magnetic Resonance Studies in Multiple Phase Systems: Lifetime of a Water Molecule in an Adsorbing Phase on Silica Gel. *J. Phys. Chem.* **1957**, *61*, 1328–1333.
70. Rafferty, J. L.; Siepmann, J. I.; Schure, M. R. The Effects of Chain Length, Embedded Polar Groups, Pressure, and Pore Shape on Structure and Retention in Reversed-Phase Liquid Chromatography: Molecular-Level Insights from Monte Carlo Simulations. *J. Chromatogr. A* **2009**, *1216*, 2320–2331.
71. Rafferty, J. L.; Zhang, L.; Siepmann, J. I.; Schure, M. R. Retention Mechanism in Reversed-Phase Liquid Chromatography: A Molecular Perspective. *Anal. Chem.* **2007**, *79*, 6551–6558.
72. Gummel, J.; Cousin, F.; Boué, F. Counterions Release from Electrostatic Complexes of Polyelectrolytes and Proteins of Opposite Charge: A Direct Measurement. *J. Am. Chem. Soc.* **2007**, *129*, 5806–5807.
73. Rosenfeldt, S.; Wittemann, A.; Ballauff, M.; Breininger, E.; Bolze, J.; Dingenouts, N. Interaction of Proteins with Spherical Polyelectrolyte Brushes in Solution as Studied by Small-Angle X-Ray Scattering. *Phys. Rev. E: Stat., Nonlinear, Soft Matter Phys.* **2004**, *70*, 061403.
74. Cormack, A. N.; Lewis, R. J.; Goldstein, A. H. Computer Simulation of Protein Adsorption to a Material Surface in Aqueous Solution: Biomaterials Modeling of a Ternary System. *J. Phys. Chem. B* **2004**, *108*, 20408–20418.
75. Langdon, B. B.; Mirhossaini, R. B.; Mabry, J. N.; Sriram, I.; Lajmi, A.; Zhang, Y.; Rojas, O. J.; Schwartz, D. K. Single-Molecule Resolution of Protein Dynamics on Polymeric Membrane Surfaces: The Roles of Spatial and Population Heterogeneity. *ACS Appl. Mater. Interfaces* **2015**, *7*, 3607–3617.
76. Mabry, J. N.; Skaug, M. J.; Schwartz, D. K. Single-Molecule Insights into Retention at a Reversed-Phase Chromatographic Interface. *Anal. Chem.* **2014**, *86*, 9451–9458.
77. Kisley, L.; Chen, J.; Mansur, A. P.; Shuang, B.; Kourentzi, K.; Poongavanam, M. V.; Chen, W. H.; Dhamane, S.; Willson, R. C.; Landes, C. F. Unified Superresolution Experiments and Stochastic Theory Provide Mechanistic Insight into Protein Ion-Exchange Adsorptive Separations. *Proc. Natl. Acad. Sci. U. S. A.* **2014**, *111*, 2075–80.
78. Sulpizi, M.; Gaigeot, M.-P.; Sprik, M. The Silica−Water Interface: How the Silanols Determine the Surface Acidity and Modulate the Water Properties. *J. Chem. Theory Comput.* **2012**, *8*, 1037–1047.
79. Wirth, M. J.; Swinton, D. J.; Ludes, M. D. Adsorption and Diffusion of Single Molecules at Chromatographic Interfaces. *J. Phys. Chem. B* **2003**, *107*, 6258–6268.
80. Kastantin, M.; Langdon, B. B.; Chang, E. L.; Schwartz, D. K. Single-Molecule Resolution of Interfacial Fibrinogen Behavior: Effects of Oligomer Populations and Surface Chemistry. *J. Am. Chem. Soc.* **2011**, *133*, 4975–4983.
81. Skaug, M. J.; Schwartz, D. K. Using the Dynamics of Fluorescent Cations to Probe and Map Charged Surfaces. *Soft Matter* **2012**, *8*, 12017–12024.
82. Honciuc, A.; Harant, A. W.; Schwartz, D. K. Single-Molecule Observations of Surfactant Diffusion at the Solution- Solid Interface. *Langmuir* **2008**, *24*, 6562–6566.
83. Kastantin, M.; Schwartz, D. K. Connecting Rare DNA Conformations and Surface Dynamics Using Single-Molecule Resonance Energy Transfer. *ACS Nano* **2011**, *5*, 9861–9869.
84. Skaug, M. J.; Mabry, J.; Schwartz, D. K. Intermittent Molecular Hopping at the Solid-Liquid Interface. *Phys. Rev. Lett.* **2013**, 110.
85. Hilyte Fluor. http://www.anaspec.com/content/pdfs/c_literature168.pdf (accessed March 1, 2015).
86. Mukhopadhyay, S.; Krishnan, R.; Lemke, E. A.; Lindquist, S.; Deniz, A. A. A Natively Unfolded Yeast Prion Monomer Adopts an Ensemble of Collapsed and Rapidly Fluctuating Structures. *Proc. Natl. Acad. Sci. U. S. A.* **2007**, *104*, 2649–2654.
87. Langdon, B. B.; Kastantin, M.; Walder, R.; Schwartz, D. K. Interfacial Protein-Protein Associations. *Biomacromolecules* **2014**, *15*, 66–74.
88. Kastantin, M.; Schwartz, D. K. Identifying Multiple Populations from Single-Molecule Lifetime Distributions. *ChemPhysChem* **2013**, *14*, 374–380.